TISSUE ENGINEERING: Part A
Volume 16, Number 9, 2010

DOI: 10.1089/ten.tea.2009.0632

The Effect of Novel Fluorapatite Surfaces on Osteoblast-Like Cell Adhesion, Growth, and Mineralization

Jun Liu, Ph.D.,[1] Taocong Jin, M.D.,[1] Syweren Chang, M.S.,[1] Agata Czajka-Jakubowska, Ph.D.,[2] Zhaocheng Zhang, Ph.D.,[1] Jacques E. Nör, Ph.D.,[1] and Brian H. Clarkson, Ph.D.[1]

There is increasing demand for biomedical implants to correct skeletal defects caused by trauma, disease, or genetic disorder. In this study, the MG-63 cells were grown on metals coated with ordered and disordered fluorapatite (FA) crystal surfaces to study the biocompatibility, initial cellular response, and the underlying mechanisms during this process. The long-term growth and mineralization of the cells were also investigated. After 3 days, the cell numbers on etched metal surface are significantly higher than those on the ordered and disordered FA surfaces, but the initial adherence of a greater number of cells did not lead to earlier mineral formation at the cell–implant interface. Of the 84 cell adhesion and matrix-focused pathway genes, an up- or down-regulation of a total of 15 genes such as integrin molecules, integrin alpha M and integrin alpha 7 and 8 was noted, suggesting a modulating effect on these adhesion molecules by the ordered FA surface compared with the disordered. Osteocalcin expression and the mineral nodule formation are most evident on the FA surfaces after osteogenic induction (OI) for 7 weeks. The binding of the ordered FA surfaces to the metal, with and without OI, was significantly higher than that of the disordered FA surfaces with OI. Most significantly, even without the OI supplement, the MG-63 cells grown on FA crystal surfaces start to differentiate and mineralize, suggesting that the FA crystal could be a simple and bioactive implant coating material.

Introduction

The response of the body to the presence of an implant is a dynamic process that starts immediately after implantation and spans many years. This process remodels the interface zone between the implant and living tissue at all dimensional levels from the molecular to the cell and tissue morphology level.[1] Immediately after clinical insertion of an implant into a patient, it becomes coated with a proteinacious layer, which is a key mediator of cell adhesion. With time the proteins will undergo certain changes (conformation, composition, etc.) at the implant surface. This will give rise to osteoinduction by the proliferation of cells and their differentiation toward bone cells, revascularization, and eventual gap closure.[2] Ideally, a strong union will be formed between the implant and the tissue. However, sometimes connective tissue is formed at the interface, resulting in a fibrous tissue capsule that prevents osteointegration and ultimately causing implant failure.

As a major component of hard tissues such as bone and teeth, hydroxyapatite (HA) [$Ca_{10}(PO_4)_6(OH)_2$] has been of interest with regard to its physicochemical properties for various biomedical applications for many years. The biological properties of HA, such as biocompatibility and bioactivity, are closely related to its chemical composition, morphology, and structure. In principle, HA itself would be a suitable bone substitute. However, the relatively low strength and toughness of HA precludes its use in these applications.[3] Consequently, it is often used as a coating for dental and orthopedic implants. The HA coating elicits a specific biological response at the interface of the implant material because of its surface chemistry, which influences the adsorption of noncollageneous proteins such as osteocalcin (OCN), osteonectin, silylated glycoproteins, and proteoglycanes. This will result in the eventual establishment of an osseoconductive union between the living tissue and the biomaterial.[4] However, the limited stability of plasma-sprayed HA with its thermal decomposition products, which are soluble in the body, has stimulated interest in bioactive materials with increased resorption resistance.[5,6] One such material is fluorapatite (FA), within which the fluoride ions replace the hydroxyl ions of the HA to create a tighter lattice structure. This increases the stability and reduces the solubility of the FA. Small amounts of fluoridated HA (FHA) exist in bone.[7] Previous studies have shown that FHA coatings with appropriate F content allow faster apatite deposition than pure HA.[8,9] The FHA coatings with different F concentrations, prepared by sol-gel method, showed good

[1]Department of Cariology, Restorative Sciences and Endodontics, Dental School, University of Michigan, Ann Arbor, Michigan.
[2]Karol Marcinkowski University of Medical Sciences, Poznan, Poland.

biocompatibility,[10] giving comparable results to that of HA for cellular attachment and alkaline phosphatase expression.[8,11,12] As a possible biomaterial for bone and tooth implants, FA has been regaining attention and has been increasingly investigated in the last 10 years for its stimulating effects in hard tissue regeneration; and for the purpose of maintaining the stability of materials during processing.[13,14] Fluoride has also been shown to suppress osteoclast maturation, inhibit phagocyte cellular activity, and reduce fibroblast proliferation.[15] Therefore, the addition of fluoride ions to a HA bone coating could further improve the union between the bone and implant and perhaps accelerate the integration process.

Oh *et al.*[16] have recently shown that a vertically aligned array of TiO_2, treated with NaOH, induced the growth of HA and that the kinetics of the HA formation was significantly accelerated by the presence of the aligned nanostructures. Chen *et al.*[17,18] have recently described two methods to synthesize FA crystals. One was under ambient conditions and produced short crystals. The other used an ethylenedeiaminetetraacetic acid (EDTA)–$Na_4.4H_2O$ to stabilize the Ca, allowing slow release of Ca^{2+} under mild hydrothermal conditions. The Chen *et al.*[17] publication shows our ability to control the composition and size of the nanorods. Further, we demonstrated a way to produce aligned FA films via this hydrothermal method. The crystals are very well aligned over a large area after being deposited on a stainless steel (SS) or titanium (Ti) surface. All the crystals had a similar growth rate, and the densely packed growth mode along the c-axis forced the rod-like crystals to align parallel to each other. Thus, highly orientated FA films were deposited on the substrate.[18] In our preliminary experiment, we have grown the FA apatite films on both the etched SS and Ti surfaces and found that the crystal composition, alignment, size, shape, and structure are the same on the two surfaces. Therefore, in this study, the SS substrates serve as cheaper metal surfaces for the FA crystal coating.

In vitro osteoblast and bone marrow stem cell culture models have been valuable tools for the biocompatibility analysis of new materials. Interaction of these cells with various biomaterials would provide valuable information establishing the relationship of material characteristics (composition, crystallinity, surface chemistry/energy, protein adsorption, etc.) with corresponding cell phenotypic behavior (adherence, proliferation, differentiation, etc.), which are fundamental to the future application of these biomaterials in the orthopedic and dental fields. For bone–implant materials, surface properties play an essential role in osteoblast adhesion onto a biomaterial surface. Enhanced adhesion and long-term activity of osteoblasts have also been reported on nano-HA surfaces.[19] The observed increase in osteoblast adhesion with the nano-HA surfaces might be related to the greater surface area exhibited by the nanomaterials, or the promotion of deposition of selective serum proteins facilitating osteoblast adhesion. However, how the HA surface characteristics affect the underlying mechanism for better cell attachment to different FA surfaces still remains unclear. Another study also found that ordered nano-HA electrochemically coated on a Ti substrate exhibited good biocompatibility although it did not explore the mechanisms involved in the cellular response.[20]

Surface-driven control of the osteoblast adhesion and long-term mineralization, which requires fabrication of favorable functional surfaces of biomaterials, would be a more attractive approach for the implantation of tissue-engineered constructs into a host. Thus, in this study FA substrates, of ordered and disordered surface organization, were used to investigate their effect on the biocompatibility, initial cellular response, long-term growth, cellular differentiation, and mineralization of the MG-63 cells. The underlying mechanisms during these processes were also studied.

Materials and Methods

Synthesis of the FA apatite surfaces

For a typical synthesis of FA crystals, 9.36 g EDTA calcium disodium salt (EDTA-Ca-Na_2) and 2.07 g $NaH_2PO_4.H_2O$ were mixed with about 90 mL distilled water. The suspensions were stirred continuously until the powder dissolved. The pH was adjusted to 6.0 using NaOH. Before mixing 0.21 g NaF in 90 mL of the EDTA-Ca-Na_2 and NaH_2PO_4 solution, it was dissolved in 10 mL water (pH 7.0) and stirred continuously. The FA crystal growth on the substrates (15 mm SS discs) was achieved by adding the discs to 100 mL of newly prepared EDT-Ca-Na_2/NaH_2PO_4/NaF mixture and then autoclaving at 121°C at pressure of 2.4×10^5 Pa for 10 h. Ordered and disordered films were produced individually in the same reaction system but on the undersurfaces and upper surfaces of the SS discs, respectively. The SS discs (TED PELLA, Inc.) are high-quality SS (alloy 430) discs originally used for Atomic Force Microscopy with smooth edges and consistently flat surfaces. The SS alloy 430 is a chromium ferrite that resists corrosion and is nonhardenable. The ordered crystal surface structure, which is very well aligned, with the C-axis of the crystals arranged perpendicular to the metal substrate, whereas the disordered FA crystal surface is composed of crystals of arranged randomly; that is, there is no well-aligned crystal structure. The detailed characterization of the two FA substrates has been investigated by transmission electron microscopy, X-ray diffraction, and energy dispersive X-ray spectroscopy in our previous publication.[18]

Cell culture and cell attachment assay

Human osteosarcoma cell line MG-63 (ATCC CRL-127) was used in this experiment. The MG-63 cells were cultured in a standard cell culture incubator at 37°C and 5% CO_2 using minimum essential medium (Eagle) supplemented with 10% fetal bovine serum, 1% penicillin–streptomycin, and 2 mM L-glutamine. Cells in confluent monolayer were harvested with trypsin–EDTA. Before cell seeding, the etched SS disc surface, and the ordered and disordered FA substrates were equilibrated with the 10% fetal bovine serum culture medium for 2 h. After being counted, harvested cells were then seeded onto 12-well cell culture plates containing different FA samples under the above serum adsorption conditions. Cells were seeded on the three sterilized surfaces at a density of 1×10^5 cells/mL and cultured for 3 days. At the end of culture period, the samples were removed and placed into new 12-well plates. After being washed twice with phosphate-buffered saline (PBS), cells were detached with trypsin–EDTA, stained with trypan blue, and then counted using a hemocytometer. Statistical analysis was carried out using one-way analysis of variance (ANOVA) and Tukey's

post hoc test with an average of 3–5 replicates from each group, and significance was considered at $p < 0.05$.

Flow cytometric analysis of initial cellular growth

Under the same preadsorption and incubation conditions as above, the MG-63 cells grown for 3 days on six discs of each of the FA surfaces were harvested and fixed with 70% cold ethanol for 30 min. Samples were washed with PBS, resuspended in 0.5 mL PI-RNAse solution, and incubated for 30 min. Samples were then subjected to flow cytometer analysis. The proliferation index (PrI, $S + G_2M$), which is defined as the percentage of cells (fraction of S phase $+ G_2$ phase $+$ M phase) in the cell cycle, of the cells grown on the ordered and disordered FA surfaces underwent statistical analysis using an unpaired *t*-test, and significance was considered at $p < 0.05$.

Scanning electron microscopy observation

After 7, 21, and 35 days of culture, the cells grown on the two FA surfaces were rinsed and fixed in 2.5% glutaraldehyde in distilled water, serially dehydrated, and critical point dried. Scanning electron microscopy (SEM) analysis was conducted on a Phillips XL30FEG scanning electron microscope (FEI company) operated at 10 kV (resolution: 2.0 nm at 30 kV, 5.0 nm at 1 kV). The SEM specimen was coated with Au/Pd film to prevent specimen charging.

RNA isolation and reverse transcription (RT)

Total cellular RNA was isolated from MG-63 cells grown for 3 days on the two surfaces using the RNeasy Mini kit (Qiagen) according to the manufacturer's instructions. RNA was treated with the RNase-free DNase Set (Qiagen) during RNA isolation.

RT^2 profiler polymerase chain reaction array analysis

In this study we focused on exploring if there was a difference on the initial cellular adhesion between the two distinctly different surface topographies. Thus, we selected the matrix and adhesion-pathway-focused polymerase chain reaction (PCR) array to compare the molecular mechanism underlying the cellular response on the two FA surfaces. Specimens were analyzed using the human pathway-focused matrix and adhesion PCR array, which combines the PCR sensitivity and the multi-gene profiling capability of a microarray. Briefly, the cDNA samples were prepared from the isolated RNA using the reverse transcription (RT) first-strand kit (Cat. No. C-03), and then added to the RT^2 quantitative PCR master mix containing SYBR Green and reference dye. The above mixture was then aliquoted across the PCR array templates, which contain 84 pathway-specific genes plus controls. The real-time PCR analysis was carried out using an ABI 7700 sequence detector (Applied Biosystems). Relative gene expression values were analyzed using the Superarray Web-based software package performing all $\Delta\Delta C_t$-based fold-change calculations.

Western blots

After osteogenic induction (OI) for 7 weeks, cells grown on the three substrate surfaces were washed with cold 1XPBS, scraped with a rubber policeman, and lysed in 1% Nonidet P-40 (NP-40) lysis buffer (50 mM Tris-HCL, pH 7.4, 200 mM NaCl, 2 mM $MgCl_2$, and 10% glycerol) containing protease inhibitors. Cell lysates were loaded in 15% sodium dodecyl sulfate–polyacrylamide gel electrophoresis gel. Membranes were incubated with mouse antihuman osteoclacin antibody at 1 to 1000 dilution (Santa Cruz Biotechnology) and mouse anti-glyceraldehyde 3-phosphate dehydrogenase at 1 to 1,000,000 dilution (Chemicon) overnight at 4°C. Affinity-purified second antibodies conjugated with horseradish peroxidase (Jackson ImmunoResearch Laboratories) were used, and immunoreactive proteins were observed by SuperSignal West Pico chemiluminescent substrate (Thermo Scientific) and exposed to X-ray film. Three separate cell lysates from the experimental substrate surfaces were used for the quantitative analysis of the optical band density of OCN expression by determining the ratio of OCN/glyceraldehyde 3-phosphate dehydrogenase using Image J program (NIH). Relative band densities were compared with the band density of control group. Triplicate samples from each experimental surfaces were used for one-way ANOVA and Tukey's *post hoc* test, and significance was considered at $p < 0.05$.

Mineralization induction

After confluency, the MG-63 cells grown on the three substrates were further cultured in the OI medium for 7 weeks, with medium changes twice per week. The minimum essential growth medium supplemented with 10 mM β-glycerophosphate, 10^{-8} M dexamethasone, and 50 μg/mL ascorbic acid (AA) was used as the OI medium.

For the above experiments, the time point for the initial cell adhesion and the PCR array was based on previous

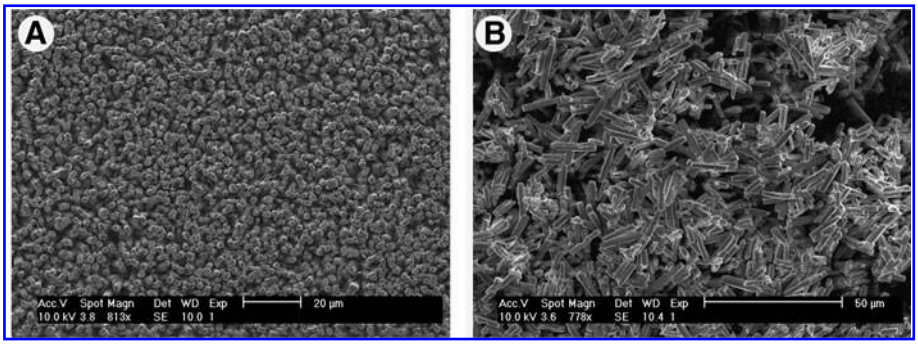

FIG. 1. Scanning electron micrograph of synthesized ordered (**A**) and disordered (**B**) FA crystal surfaces. Ordered and disordered films were produced individually on the undersurfaces and upper surfaces of the SS discs. FA, fluorapatite; SS, stainless steel.

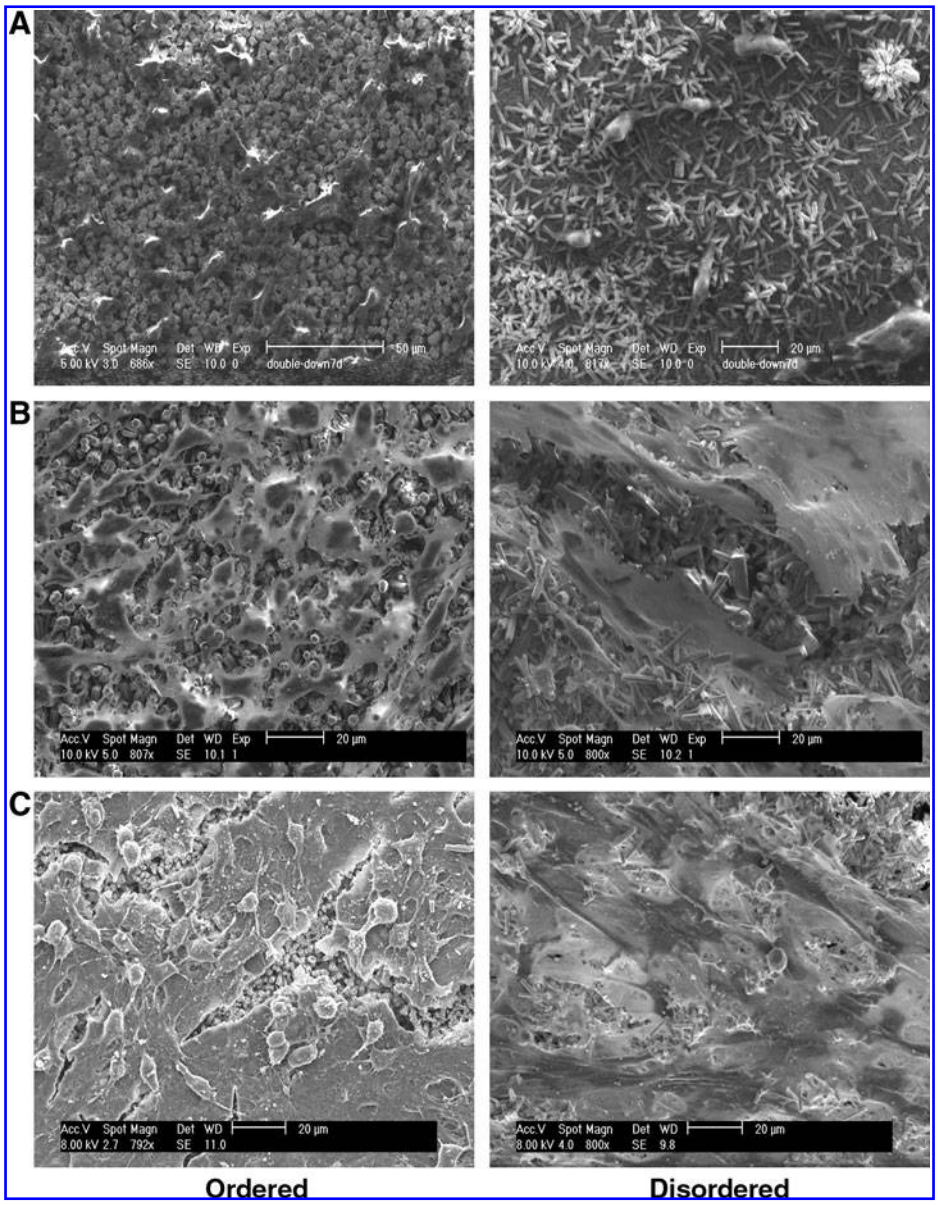

FIG. 2. Scanning electron micrograph of MG-63 cells grown on FA surfaces for 1 week (**A**), 3 weeks (**B**), and 5 weeks (**C**).

studies.[21] The time points for the long-term growth of the MG-63 cells were chosen based on our preliminary studies that showed distinct morphological changes at the selected times points of 1, 3, and 5 weeks. The times point for the mineralization was based on our preliminary study and previous studies that showed that mineralization occurred after the cells had been induced for 48 days.

Nanoscratch test

After the OI for 7 weeks, the MG-63 cell layer was mechanically removed and the extracellular matrix (ECM) further treated with the protein extraction buffer NP-40. The samples of the disordered FA crystal surfaces with OI, and ordered FA crystal surfaces with and without OI were used for the nanoscratch test. No tests were conducted on the samples of disordered FA surfaces without OI and the SS surfaces either with or without OI, since the surface layers were easily removed after the cells and the protein were desorbed. Briefly, the samples were tested using the Nanoscratch Tester from CSM instruments (software version 3.87.09). The test conditions and parameters were set up using the progressive load rate of 375 mN/min and the scanning load of 2.5 mN, with the initial load of 2.5 mN and the final load of 125 mN; the scratch length was 0.98 mm with a speed of 3 mm/min. The Rockwell diamond of the 10 μm radium indenter was applied to the surface of the samples. For each sample, the critical load at which damage of the coating occurred was measured. Triplicate samples from each FA surfaces were used for one-way ANOVA and Tukey's *post hoc* test, and significance was considered at $p < 0.05$.

Results

SEM observation

SEM of synthesized ordered and disordered FA crystal surfaces showed that the crystals were very well aligned, with the C-axis of the crystals perpendicular to the metal substrate,

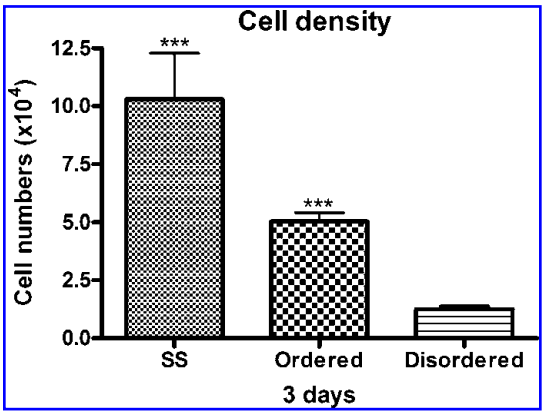

FIG. 3. Cell density on etched SS surface, and ordered and disordered FA surfaces. Statistical analysis was carried out using one-way ANOVA and Tukey's *post hoc* test with an average of 3–5 replicates from each group, and significance was considered at $p < 0.05$. The initial attached cell numbers on the etched SS surfaces were significantly higher than that on the ordered and the disordered FA surfaces. The cell density on the ordered FA surfaces were also significantly higher than that on the disordered (***, $p < 0.01$.) ANOVA, analysis of variance.

over a large area after being deposited on the undersurface of the SS discs (Fig. 1A). The FA crystals grown on the upper surface of the SS discs were randomly arranged without forming the well-aligned structure (Fig. 1B). SEM of the MG-63 cells grown on both the ordered and disordered FA crystal surfaces spread well and flattened, demonstrating the good biocompatibility of both surfaces. However, a greater number of cells were identified on the ordered FA crystal surface compared with the disordered surface after cell growth of 1 week (Fig. 2A). At greater magnification when grown on ordered FA crystal surfaces, cytoplasmic extensions from the MG-63 cells adhering to the individual FA crystals could be seen (data not shown). At 14 days, the cells had more polygonal shape and attached to the substrate surfaces through cellular extensions (data not shown). After culturing for 21 days, dense cell nodule formation was observed on ordered FA surface with more cellular extensions and ECM, whereas isolated or fused cell nodules were seen on the disordered FA surface (Fig. 2B). At 35 days, the cells were fused together to completely cover the FA surfaces with a denser matrix on the ordered FA surfaces than the disordered. The ordered FA crystal surface can be seen beneath the cell–matrix layer, which split during the SEM sample processing (Fig. 2C).

Table 1. Cell Cycle Analysis of the MG-63 Cells Grown for 3 Days on Ordered and Disordered Fluorapatite Surfaces (%)

	G1	*S*	*G_2M*	*PrI ($S+G_2M$)*	*Apoptosis*
Ordered FA	46.51	30.65	22.85	53.50	0.01
Disordered FA	39.99	34.85	25.17	60.02	0.00

The proliferation index (PrI, $S+G_2M$) of the cells grown on the ordered and disordered FA surfaces was statistically analyzed using unpaired *t*-test, and significance was considered at $p < 0.05$.
FA, Fluorapatite.

Cell density on ordered and disordered FA surfaces

The initial attached MG-63 cell numbers on the etched SS surfaces were significantly higher than that on the ordered and the disordered FA surfaces after cells were grown for 3 days (one-way ANOVA and Tukey's *post hoc* test, $p < 0.01$, $n = 3$). The cell density on the ordered FA surfaces was also significantly higher than that on the disordered (one-way ANOVA and Tukey's *post hoc* test, $p < 0.05$, $n = 3$) (Fig. 3).

Flow cytometric analysis of initial cellular growth

The proliferation index (PrI, $S+G_2M$) of the cells grown for 3 days on the ordered and disordered FA surfaces was 53.5% and 60.0%, respectively. No significant difference was found between the PrI of the cells grown on these two surfaces ($p > 0.05$) (Table 1).

Human matrix and adhesion-pathway-focused PCR array analysis

Of the 84 focused pathway genes, a total of 15 genes were either up- or downregulated in the cells on the ordered FA surface compared with the disordered surface. Of the cell adhesion molecules, the upregulation of versican, hyaluronan synthase 1, integrin alpha M (*ITGAM*), and selectin L was coordinated with the downregulation of *ITGA* 7 and 8, laminin alpha 2, catenin delta 2, and platelet/endothelial cell adhesion molecule. Among the ECM proteases, the upregulation of the matrix metalloproteinases 10 and 13 and A disintegrin and metalloproteinase (ADAM) metallopeptidase with thrombospondin type 1 motif 8 corresponded with the downregulation of 3 other metallopeptidases (Fig. 4, Table 2).

Western blots

After OI for 7 weeks, the relative optical band density analysis showed OCN expression being significantly higher in cells grown on disordered FA surfaces with and without OI compared to ordered FA surfaces either with or without the OI and SS surfaces with OI. No OCN expression was detected in the cells grown on SS surfaces without OI or in the control group where the band density was arbitrarily adjusted to the value of one (Figs. 5 and 6).

Mineralization induction

After the OI for 7 weeks, the MG-63 cell layer was mechanically removed and further treated with the protein extraction buffer NP-40; the resulting samples were processed for SEM examination. More densely deposited amorphous mineral nodules were observed on the ordered FA crystal surfaces without (Fig. 7A) and with (Fig. 7B) OI. Obvious mineral nodule formation could also be seen on the disordered (Fig. 7C) FA crystal surfaces. No SEM pictures were taken of the samples of disordered FA surfaces without OI and the SS surfaces either with or without OI, since the surface layers were easily removed after the cells had been removed and the protein extracted (Fig. 7).

Nanoscratch test

The critical loads applied to the bio-processed FA surfaces were as follows: ordered FA surfaces with OI at 88.27 ± 4.24,

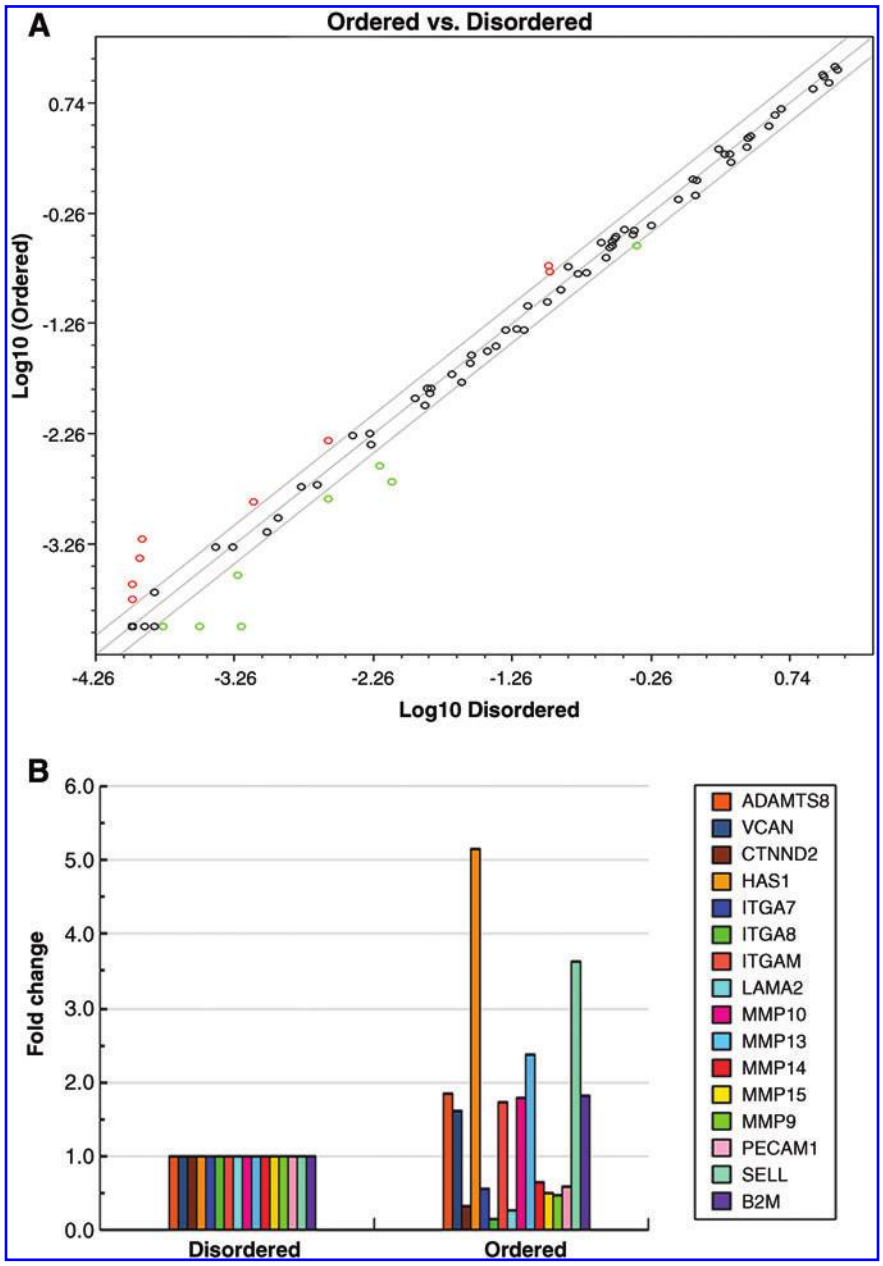

FIG. 4. (**A**) Scatter plot of expression of human extracellular matrix and adhesion molecules on ordered FA surfaces compared with disordered FA surfaces. The boundary value is 1.5. (**B**) Bar graph of expression of human extracellular matrix and adhesion molecules on ordered FA surfaces compared with disordered FA surfaces. Color images available online at www.liebertonline.com/ten.

ordered FA surfaces without OI at 103.76 ± 5.27, and the disordered FA surfaces with OI at 28.16 ± 8.7. The critical loads to delaminate the ordered FA surfaces with and without OI were significantly higher than that of the disordered FA surfaces with OI ($p < 0.05$); there was no significant difference of the critical loads between the two ordered FA surfaces (Fig. 8).

Discussion

There is already a global demand for biomedical implants to correct skeletal defects caused by trauma, disease, or genetic disorder. It has been reported that in the United States alone, some 910,000 dental implants, 500,000 hip and knee prostheses, and 60,000 cochlear implants are implanted annually, and that the implant rate is growing at 10%–11% per year for the world market.[22] In this study, we first investigated the initial cellular response of MG-63 cells to ordered and disordered FA surfaces and explored the mechanisms underlying this initial cellular adhesion process, to provide valuable information on the biocompatibility of these newly developed novel biomedical materials.

Adhesion of anchorage-dependent mammalian cells is usually divided into at least four major steps that precede proliferation: protein adsorption, cell–substratum contact, cell–substratum attachment, and cell adhesion/spreading. Recent advances in biomaterials have focused on the synthesis of new materials with tailored surface modifications for promoting certain characteristics that regulate biocompatibility. Correlations among surface properties, protein adsorption, and cell response therefore have been of great interest to the biomedical material researchers. Generally, surface–protein interactions rapidly produce a proteinaceous conditioning layer that determines the nature of subsequent cell surface behavior. Therefore, initial protein adhesion plays a major role in determining the biocompatibility of materials.

Table 2. Fold-Change of the Human Extracellular Matrix and Adhesion Molecules Expressed by the MG-63 Cells Grown on the Ordered Fluorapatite Surface Relative to the Disordered Surface

Symbol	*Unigene*	*Refseq*	*Gname*	*Fold change*
HAS1	Hs.57697	NM_001523	HAS	5.16
SELL	Hs.82848	NM_000655	CD62L/LAM-1	3.63
MMP13	Hs.2936	NM_002427	CLG3	2.36
ADAMTS8	Hs.271605	NM_007037	ADAM-TS8/METH2	1.84
MMP10	Hs.2258	NM_002425	SL-2/STMY2	1.79
ITGAM	Hs.172631	NM_000632	CD11B/CR3A	1.73
VCAN	Hs.643801	NM_004385	CSPG2/DKFZp686K06110	1.60
ITGA8	Hs.171311	NM_003638	Integrin a8	−6.24
LAMA2	Hs.200841	NM_000426	LAMM	−3.66
CTNND2	Hs.314543	NM_001332	GT24/NPRAP	−3.14
MMP9	Hs.297413	NM_004994	CLG4B/GELB	−2.18
MMP15	Hs.80343	NM_002428	MT2-MMP/MTMMP2	−2.02
ITGA7	Hs.524484	NM_002206	FLJ25220	−1.82
PECAM1	Hs.514412	NM_000442	CD31/PECAM-1	−1.70
MMP14	Hs.2399	NM_004995	MMP-X1/MT1-MMP	−1.56

After the real-time polymerase chain reaction amplification, relative gene expression values were analyzed using the Superarray Web-based software package performing all $\Delta\Delta C_t$-based fold-change calculation.
Refseq, reference sequence; Gname, gene name.

Proteins adsorbed in different quantities, densities, conformations, and orientations depend on the chemical and physical characteristics of the surface involving van der Waals forces and hydrophobic and electrostatic interactions. Adsorbed proteins may act as mediators for cell adhesion if they have the correct geometry (i.e., exposed Arg-Gly-Asp [RGD] sequence in fibronectin [FN]) to mediate cell attachment.[23] Studies have shown the importance of the compositional change of the adsorbed protein layer in determining cellular response to biomaterials. In this study, the initial cellular attachment of the MG-63 cells was significantly higher on the ordered than on the disordered FA surfaces, although both surfaces showed excellent biocompatibility, as indicated in the flow cytometric analysis, which showed an almost 0% apoptosis rate of cells on both surfaces. Thus, the composition and conformation of the favorably adsorbed protein layer might be responsible for the enhanced MG-63 cellular response on the ordered FA surfaces. Cell–surface interactions have been shown to be affected by underlying surface chemistry, whereas neither the structural or topographical effects on surface bound protein conformations and geometries governing cell adhesion have been fully elucidated.[23]

After protein adsorption, there are usually two kinds of adhesion of cells: one is a physical bond between the cells,

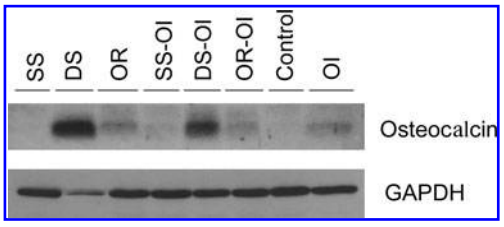

FIG. 5. Western blots of OCN expression of the MG-63 cells grown on the etched SS surface, and disordered (DS) and ordered (OR) FA crystal surfaces with or without the OI. Control: the MG-63 cells grown on culture dish surface without OI. OI: the MG-63 cells grown on culture dish surface with OI. OCN, osteocalcin; OI, osteogenic induction.

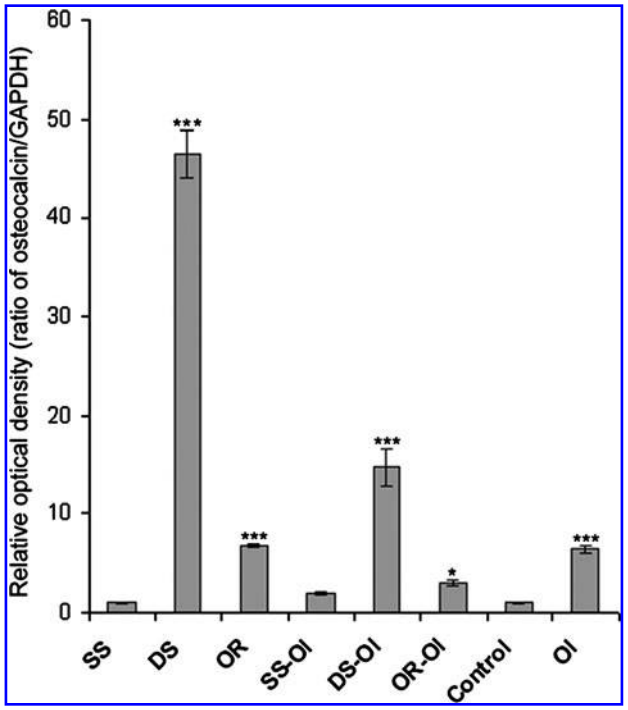

FIG. 6. Quantitative analysis of the optical band density of OCN expression by the ratio of OCN/GAPDH using Image J program (NIH). Triplicate samples from each experimental surface were used for one-way ANOVA and Tukey's *post hoc* test, and significance was considered at $p < 0.05$. The relative optical band density of OCN expression was significantly higher in cells grown on disordered FA surfaces with and without OI compared to ordered FA surfaces either with or without the OI and SS surfaces with OI (***, $p < 0.01$). Compared to cells grown on SS surfaces and culture dish surface, significantly higher optical band densities were also seen on ordered FA surface without OI (***, $p < 0.01$) and on ordered FA surface with OI (*, $p < 0.05$) Control: the MG-63 cells grown on culture dish surface without OI. OI: the MG-63 cells grown on culture dish surface with OI. GAPDH, glyceraldehyde 3-phosphate dehydrogenase.

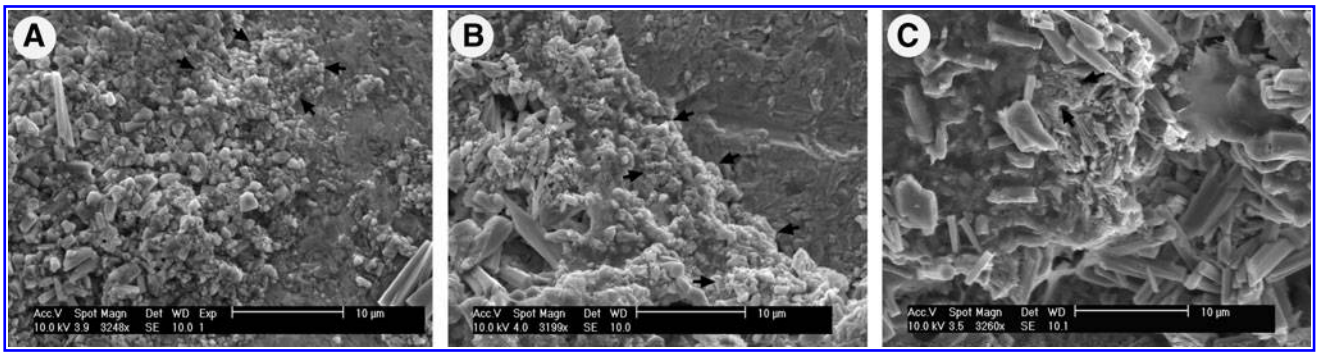

FIG. 7. Scanning electron micrograph of the mineral nodule formation on ordered and disordered FA crystal surfaces after the OI for 7 weeks. More densely deposited amorphous mineral nodules were observed on the ordered FA crystal surfaces without (**A**) and with (**B**) OI; obvious mineral nodule formation could also be seen on the disordered (**C**) FA crystal surface (dark arrows).

that is, cell–cell adhesion formed among adjacent cells, and the other is the cell–matrix adhesion, involving the cell–matrix interactions that control cell adhesion, cell survival, and the cellular proliferation and differentiation process. Adsorption of adhesion proteins, such as FN and vitronectin, has been reported to mediate cell adhesion.[24] FN is one of many known ECM proteins that, along with vitronectin, fibrinogen, collagens, laminin, osteopontin, and other trace proteins, mediate the specific interaction of cells to surfaces via cell integrin receptors. A previous study revealed that FN could be conformationally activated by surface adsorption, and this surface activation might be due to the exposure of its RGD sequences.[25] In plasma or solution as well as on the surface of cells, under normal physiological conditions, FN appears to be in a globular or compact form; FN is found in the flexible and extended form when being incorporated into ECM and then self-associates into a dense fibrillar network.[25]

The integrin-mediated interaction of cells with the ECM involves the formation of focal contacts or formation of focal adhesions along the plasma membrane. In this study, after the growth of MG-63 cells on the two surfaces for 3 days, expression of human pathway-focused matrix and adhesion molecules of the cells were analyzed using PCR array. This time point was chosen because if the gene studies are applied too early, the cell will not have sensed the interfacial environment; if applied too late, the cell will have had enough time to remodel the pericellular environment to give inaccurate adhesion information.[21] In this study, expression of integrin family members *ITGAM*, and *ITGA* 7 and 8 were significantly different between cells grown on the two surfaces. This suggests that these integrin members probably play major roles in the initiation of conformational activation of FN outside of the cells and the organization of the actin cytoskeleton inside the cells, which eventually leads to the active FN fibril formation for cell attachment. The coordination of other cell adhesion molecules, versican, hyaluronan synthase 1, selectin L, laminin alpha 2, catenin delta 2, and platelet/endothelial cell adhesion molecule, together with the ECM proteases, such as the matrix metalloproteinases 10 and 13 and ADAM metallopeptidase with thrombospondin type 1 motif 8, also appears to be important in establishing the favorable microenvironment (i.e., favorable focal adhesion) for the cells grown on the ordered FA surfaces. A number of intracellular signaling molecules, including focal adhesion kinase, p44/42, extracellular-signal-regulated kinase (ERK 1/2), Ras, and Src, are also involved in the formation of focal adhesions. Meanwhile the cell itself also expresses certain ECM and signaling molecules in response to the reciprocal interactions.[26]

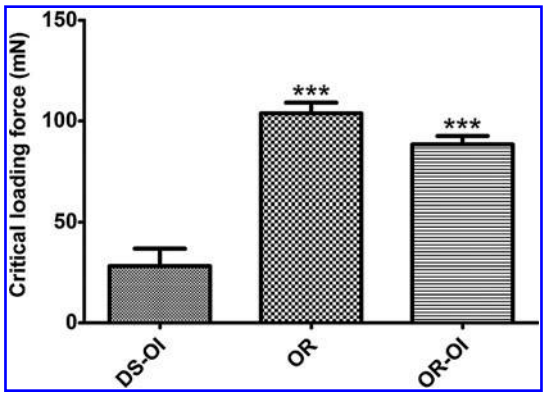

FIG. 8. Nanoscratch test on the bio-processed FA crystal surfaces. Triplicate samples from each FA surfaces were used for one-way ANOVA and Tukey's *post hoc* test, and significance was considered at $p < 0.05$. The critical loads to delaminate the ordered FA surfaces with and without OI were significantly higher than that of the disordered FA surfaces with OI (***, $p < 0.01$).

The long-term growth of the MG-63 cells on the two surfaces was achieved and observed by SEM. After culturing for 3 weeks, dense cell nodule formation was observed on the ordered FA surface with more cellular extensions and ECM, whereas isolated or fused cell nodules appeared on the disordered FA surface. At 35 days, the cells were fused together to completely cover the FA surfaces with denser matrix formation occurring on the ordered FA surfaces. However, it was reported that the MG-63 cells exhibited a round morphology, indicating cell death, when grown on the electrodeposited calcium phosphate surfaces after 28 days of culture.[27]

In general, the first phase of cell–material interaction involving attachment, adhesion, and spreading of the cell may probably influence the second phase of the interaction, which is critical in bony defect repair and wound healing involving proliferation and differentiation of bone-forming cells.[28] In

our study, however, though the cell numbers on etched SS surface are significantly higher than those on the ordered and disordered FA surfaces, OCN expression, serving as a phenotypic marker of the osteoblast terminal differentiation, and the mineral nodule formation are most evident on the FA surfaces. This would indicate that the most favorable surfaces for the initial cellular adhesion might not necessarily result in favorable or the expected cell fate selection or differentiation pathways. In our experiment, the characteristics of the FA crystals and/or the topography of the FA crystal surfaces appeared to dominate the continued cell differentiation and mineralization process. Interestingly, significantly higher OCN expression was found on the disordered FA crystal surfaces either with or without the OI. This may be because more OCN was retained in the more densely deposited mineral nodules and matrix layers on the ordered FA crystal surfaces; thus, less amount of OCN was being retrieved from the total protein collections. Since OCN, one of the most abundant, noncollagenous proteins found in mineralized adult bone, binds strongly with the mineral crystal in a calcium-dependent manner.[29] However, the significantly different initial cellular adhesion, and expression of matrix and adhesion molecules results in the reestablishment of a different microenvironment during the interaction of the cells with ordered and disordered crystal surfaces. This could be attributed to differences in the mineralizing abilities of the MG-63 cells grown on the two crystal surfaces. The nano-scratch test consists of the generation of scratches with a spherical stylus, generally a diamond tip, which is drawn across the sample's surface at a constant speed and a defined normal force (constant or progressively increasing), for a defined distance. During the scratch test, the critical loads to delaminate the coatings are visually identified under the microscope after each scratch. The critical loads that are needed to expose the underlying substrate largely depend on the mechanical strength (adhesion and cohesion) of a coating–substrate composite.[30] This quantitative measurement of the mechanical strength between the bio-processed FA surfaces and the metal surface correlates with the strength of binding and integration of the mineralized matrix with the metal surfaces. The binding of these bio-processed ordered FA crystals to the SS surfaces were significantly stronger than that of the disordered crystals. After the protein extraction and cell removal from the surfaces, we have also observed densely deposited mineral nodules on the ordered FA surfaces. Therefore, the ordered FA crystals show promise as a robust and effective implant surface coating material, which may lead to the establishment of a bio-coating implant system.

In our studies, one of the most interesting findings was that, even without the OI supplement, the MG-63 cells grown on FA crystal surfaces start to differentiate into mineral-producing cells. This is very promising for the future application of the FA crystal as a simple but bioactive implant-coating material. In previous studies, the OI effects of the HA had also been observed using human pulp fibroblasts[31] and mesenchymal stem cells.[32,33] It was suggested that the HA played this role by recruiting certain growth factors to create an osteoinductive microenvironment.[33] The HA could also communicate and interact with the stem cells by generating potent inductive factors, which in turn induced the stem cells to differentiate into the osteoblast-like cells, and this inductive effect was not dependant on the upregulation of the *Cbfa1* contrary to that seen for bone morphogenetic protein (BMP).[33] In our study, not only the material itself, but also the surface topography of the FA crystals affected the differentiation and further mineralization of the MG-63 cells. The underlying mechanism during the differentiation and mineralization process needs to be further investigated. This may be explored by using the pathway-focused osteogenesis PCR array, which will enhance our understanding of the role of the micro-environment on cell differentiation and mineralization.

In accordance with our study, others have reported that, although exhibiting greater alkaline phosphatase (ALP) activity and OCN production on rough machined Ti surfaces than on smooth Ti surfaces, the MG-63 cells were unable to form mineralized nodules on either surfaces under OI.[34] Further, no mineral nodule formation occurred when MG-63 cells were grown on mineral trioxide aggregate surfaces upon OI.[35] The formation of a carbonated (bone-like) apatite layer on a material's surface appears to be essential for successful *in vivo* bone growth.[36] Further, the effect of AA on the osteoblast (specifically the MG-63 cells) differentiation is still controversial. Son *et al*. reported that AA stimulated the osteoblastic differentiation of the MG-63 cells through increased ALP activity[37]; in another study, the supplement of AA strongly inhibited the MG-63 cell mineralization in a dose-dependent manner.[38] Further studies need to be carried out to elucidate the role of AA on the MG-63 cell mineralization grown on the FA surfaces.

Different biomaterial surfaces have been shown to not only make changes in focal adhesion and ECM production but also affect the differentiation of human bone marrow mesenchymal stem cell, both in the presence and in the absence of biological stimuli. The *in vivo* biocompatibility (such as inflammation status) of the two surfaces and the integration and healing of these FA surfaces with the existing bone *in vivo* need to be further elucidated.

Acknowledgment

This work was supported by grant DE015599 from the National Institutes of Health.

Disclosure Statement

No competing financial interests exist.

References

1. Kasemo, B., and Lausmaa, J. The biomaterial-tissue interface and its analogues in surface science and technology. In: David, J.E., ed. The Bone–Biomaterials Interface. Toronto: University of Toronto Press, 1991, p. 19.
2. Hench, L.L. Biomaterials: a forecast for the future. Biomaterials **19,** 1419, 1998.
3. De Aza PN, D.A.A., and De Aza, S. Crystalline bioceramic materials. Bol Soc Esp Ceram **44,** 135, 2005.
4. Steflik, D.E., Corpe, R.S., Young, T.R., Sisk, A.L., and Parr, G.R. The biologic tissue responses to uncoated and coated implanted biomaterials. Adv Dent Res **13,** 27, 1999.
5. Fazan, F., and Marquis, P.M. Dissolution behavior of plasma-sprayed hydroxyapatite coatings. J Mater Sci Mater Med **11,** 787, 2000.
6. Heimann, R.B. Thermal spraying of biomaterials. Surface Coatings Technol **201,** 2012, 2006.

7. Pullen, L.J., and Gross, K.A. Dissolution and mineralization of sintered and thermally sprayed hydroxy-fluoroapatites. J Mater Sci Mater Med **16,** 399, 2005.
8. Kim, H.W., Kim, H.E., and Knowles, J.C. Fluor-hydroxyapatite sol-gel coating on titanium substrate for hard tissue implants. Biomaterials **25,** 3351, 2004.
9. Cheng, K., Weng, W., Qu, H., Du, P., Shen, G., Han, G., Yang, J., and Ferreira, J.M. Sol-gel preparation and *in vitro* test of fluorapatite/hydroxyapatite films. J Biomed Mater Res B Appl Biomater **69,** 33, 2004.
10. Cheng, K., Weng, W., Wang, H., and Zhang, S. *In vitro* behavior of osteoblast-like cells on fluoridated hydroxyapatite coatings. Biomaterials **26,** 6288, 2005.
11. Cavalli, M., Gnappi, G., Montener, A., Bersani, C., Lottici, P.P., Karciulis, S., Mattogno, G., and Fini, M. Hydroxy- and fluorapatite films on Ti alloy substrates: sol-gel preparation and characterization. J Mater Sci **36,** 3253, 2001.
12. Montanaro, L., Arciola, C.R., Campoccia, D., and Cervellati, M. *In vitro* effects on MG63 osteoblast-like cells following contact with two roughness-differing fluorohydroxyapatite-coated titanium alloys. Biomaterials **23,** 3651, 2002.
13. Gross, K.A., and Rodriguez-Lorenzo, L.M. Sintered hydroxy-fluorapatites. Part I: sintering ability of precipitated solid solution powders. Biomaterials **25,** 1375, 2004.
14. FN, O. Microstructure and mechanical properties of sintered enamel hydroxyapatite. Ceram Int **33,** 1309, 2007.
15. Sakae, T., Hoshino, K., Fujimori, Y., Kozawa, Y., and LeGeros, R.Z. *In vitro* interactions of bone marrow cells with carbonate and fluoride containing apatites. Key Eng Mat **192,** 347, 2001.
16. Oh, S.H., Finones, R.R., Daraio, C., Chen, L.H., and Jin, S. Growth of nano-scale hydroxyapatite using chemically treated titanium oxide nanotubes. Biomaterials **26,** 4938, 2005.
17. Chen, H., Sun, K., Tang, Z., Law, R.V., Mansfield, J.F., Czajka-Jakubowska, A., and Clarkson, B.H. Synthesis of fluorapatite nanorods and nanowires by direct precipitation from solution. Cryst Growth Des **6,** 1504, 2006.
18. Chen, H.F., Tang, Z., Liu, J., Sun, K., Chang, S.R., Peters, M.C., Mansfield, J.F., Czajka-Jakubowska, A., and Clarkson, B.H. Acellular synthesis of a human enamel-like microstructure. Adv Mater **18,** 1846, 2006.
19. Webster, T.J., Ergun, C., Doremus, R.H., Siegel, R.W., and Bizios, R. Enhanced functions of osteoblasts on nanophase ceramics. Biomaterials **21,** 1803, 2000.
20. Hu, R., Lin, C.J., and Shi, H.Y. A novel ordered nano hydroxyapatite coating electrochemically deposited on titanium substrate. J Biomed Mater Res A **80,** 687, 2007.
21. Liu, X., Lim, J.Y., Donahue, H.J., Dhurjati, R., Mastro, A.M., and Vogler, E.A. Influence of substratum surface chemistry/energy and topography on the human fetal osteoblastic cell line hFOB 1.19: phenotypic and genotypic responses observed *in vitro*. Biomaterials **28,** 4535, 2007.
22. Malchesky, P.S. Artificial organs begins 30th year of publication. Artif Organs **30,** 5, 2006.
23. Roach, P., Farrar, D., and Perry, C.C. Interpretation of protein adsorption: surface-induced conformational changes. J Am Chem Soc **127,** 8168, 2005.
24. Steele, J.G., Dalton, B.A., Johnson, G., and Underwood, P.A. Adsorption of fibronectin and vitronectin onto Primaria and tissue culture polystyrene and relationship to the mechanism of initial attachment of human vein endothelial cells and BHK-21 fibroblasts. Biomaterials **16,** 1057, 1995.
25. Aota, S., Nomizu, M., and Yamada, K.M. The short amino acid sequence Pro-His-Ser-Arg-Asn in human fibronectin enhances cell-adhesive function. J Biol Chem **269,** 24756, 1994.
26. Allen, L.T., Tosetto, M., Miller, I.S., O'Connor, D.P., Penney, S.C., Lynch, I., Keenan, A.K., Pennington, S.R., Dawson, K.A., and Gallagher, W.M. Surface-induced changes in protein adsorption and implications for cellular phenotypic responses to surface interaction. Biomaterials **27,** 3096, 2006.
27. Richard, D., Dumelie, N., Benhayoune, H., Bouthors, S., Guillaume, C., Lalun, N., Balossier, G., and Laurent-Maquin, D. Behavior of human osteoblast-like cells in contact with electrodeposited calcium phosphate coatings. J Biomed Mater Res B Appl Biomater **79,** 108, 2006.
28. Ismail, F.S., Rohanizadeh, R., Atwa, S., Mason, R.S., Ruys, A.J., Martin, P.J., and Bendavid, A. The influence of surface chemistry and topography on the contact guidance of MG63 osteoblast cells. J Mater Sci Mater Med **18,** 705, 2007.
29. Hoang, Q.Q., Sicheri, F., Howard, A.J., and Yang, D.S. Bone recognition mechanism of porcine osteocalcin from crystal structure. Nature **425,** 977, 2003.
30. Steinmann, P.A., Tardy, Y., and Hintermann, H.E. Adhesion testing by the scratch test method: the influence of intrinsic and extrinsic parameters on the critical load. Thin Solid Films **154,** 333, 1987
31. Tsukamoto, Y., Fukutani, S., Shin-Ike, T., Kubota, T., Sato, S., Suzuki, Y., and Mori, M. Mineralized nodule formation by cultures of human dental pulp-derived fibroblasts. Arch Oral Biol **37,** 1045, 1992.
32. Ohgushi, H., Dohi, Y., Tamai, S., and Tabata, S. Osteogenic differentiation of marrow stromal stem cells in porous hydroxyapatite ceramics. J Biomed Mater Res **27,** 1401, 1993.
33. Lin, L., Chow, K.L., and Leng, Y. Study of hydroxyapatite osteoinductivity with an osteogenic differentiation of mesenchymal stem cells. J Biomed Mater Res **89,** 326, 2009.
34. Schwartz, Z., Lohmann, C.H., Oefinger, J., Bonewald, L.F., Dean, D.D., and Boyan, B.D. Implant surface characteristics modulate differentiation behavior of cells in the osteoblastic lineage. Adv Dent Res **13,** 38, 1999.
35. Perez, A.L., Spears, R., Gutmann, J.L., and Opperman, L.A. Osteoblasts and MG-63 osteosarcoma cells behave differently when in contact with ProRoot MTA and White MTA. Int Endod J **36,** 564, 2003.
36. Olivares, R., Rodil, S.E., and Arzate, H. Osteoinduction properties of graphite-like amorphous carbon films evaluated *in vitro*. Diamond Relat Mater **16,** 1858, 2007.
37. Son, E., Do, H., Joo, H.M., and Pyo, S. Induction of alkaline phosphatase activity by L-ascorbic acid in human osteoblastic cells: a potential role for CK2 and Ikaros. Nutrition **23,** 745, 2007.
38. Takagishi, Y., Kawakami, T., Hara, Y., Shinkai, M., Takezawa, T., and Nagamune, T. Bone-like tissue formation by three-dimensional culture of MG63 osteosarcoma cells in gelatin hydrogels using calcium-enriched medium. Tissue Eng **12,** 927, 2006.

Address correspondence to:
Brian H. Clarkson, Ph.D.
Department of Cariology, Restorative Sciences, and Endodontics
Dental School
University of Michigan
1011 N. University Ave.
Ann Arbor, MI 48109

E-mail: bricla@umich.edu

Received: September 20, 2009
Accepted: April 22, 2010
Online Publication Date: June 8, 2010

This article has been cited by:

1. J. Liu, T. C. Jin, S. Chang, A. Czajka-Jakubowska, B. H. Clarkson. 2010. Adhesion and growth of dental pulp stem cells on enamel-like fluorapatite surfaces. *Journal of Biomedical Materials Research Part A* n/a-n/a. [CrossRef]